ORIGINAL PAPER

Comparative analysis of single-coil and double-coil active magnetic bearings for high-speed application

S. Debnath[1] · U. Das[2] · P. K. Biswas[2]

Abstract

This article compares the single- and double-coil-based active magnetic bearing (AMB) for high-speed application. Present days high-speed rotating machines have vast applications for domestic and industrial purposes. Magnetic bearing supports the load using levitation, which means contact friction is zero, so losses will be very less, and supports very high rpm. This manuscript contains the design of single- and double-coil I-type actuators, magnetic analysis using finite element-based software, simulation, experimental verification, and the high-speed test comparison between the designed systems. The magnetic analysis is performed in ANSYS Maxwell software according to the design data; similarly, simulation is also done in Multisim. After getting the required magnetic analysis data and simulation data, both the AMB designs are implemented in hardware, and the results are compared. For the high-speed test minimum, 10 V and a maximum of 100 V are applied to both AMB rotational systems and a maximum 22425 rpm speed is observed in the tachometer.

Keywords Active magnetic bearing · Controllers · Hardware implementation · I-type actuator · Magnetic analysis · Sensors · And simulation

1 Introduction

The relative position of a rotating assembly (rotor) to a fixed component(stator) is maintained by a magnetic bearing that employs electromagnetic forces. In reaction to forces produced by machine operation, a modern electronic control system modifies these electromagnetic forces. The advantages of a magnetic bearing include increased safety, environmental advantages, and the elimination of ancillary equipment due to the removal of the oil system, optimized rotor dynamic control, variable speed operation, inherent diagnostic capabilities, low energy consumption, including the possibility of outdoor installations [1].

As illustrated in Fig. 1, they are made up of several unique components: the bearing itself or the rotor, the electromagnetic coil or the actuator, the electronic control system that comprises a sensor, transducer, power amplifier, and specific controller assembly, and finally the auxiliary bearings. By adjusting the current flowing through the electromagnets, the electronic control system aims to regulate the rotor's position [2]. The machines own disturbance frequency can be taken into account while adjusting and adapting the electronic control system. Due to changes in processes, this information can be used to alter and optimize performance [3–5].

Numerous studies have been conducted to manage AMB operation and obtain an appropriate bearing action. In 2016, Zansong Fu et al. showed the process for designing four-axis magnetic bearings and the control mechanism for a high-speed motor with a 200 kW/40000 rpm design. The actuator of the magnetic bearings is designed using the analytical method as well as the finite element analysis (FEA) method [6]. In 2016, Marcel Schuck et al. explained several novel ideas for bearing less machines with extremely high rotating speeds reaching 25 million rotations per minute [7]. Alexander Smirnov et al. in 2017 provides a strategy for designing an HS electrical machine backed by AMBs that takes into account how each affects the other's impact on system performance. Development of the optimization process considers both the electrical machine and bearing designs [1]. In the study of Emil Kurvinen et al. in 2021, a modular, multi-megawatt (MMW) HSIM with three radial active magnetic

✉ U. Das
upama.eee@nitmz.ac.in

1   Department of Artificial Intelligence and Data Science, Sharad Institute of Technology College of Engineering, Yadrav, Kolhapur, Maharashtra, India

2   Department of Electrical Engineering, National Institute of Technology Mizoram, Aizawl, India
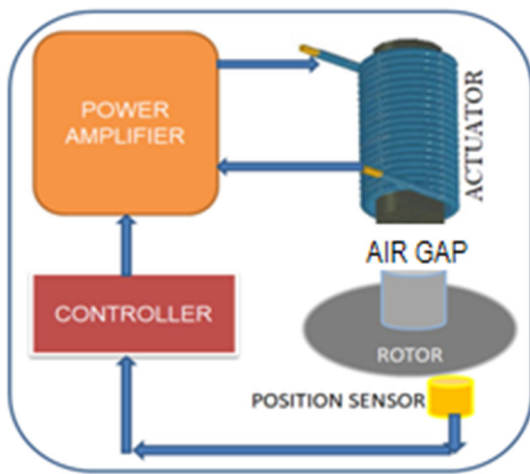
Fig. 1 Basic diagram of AMB

Table 1 Design data of single-coil and double-coilAMB

Constraints	Details
Single-coil AMB	
Maximum force	69.75 N
Rotor mass	59gm
Air gap	3 mm
Control current	3A
No of turns of actuator coil	750 T
No of turns of AC magnet coil	700 T
Double-coil AMB	
Maximum force	52.26 N
Rotor mass	66gm
Air gap	3 mm
Control current	3A
No of turns of actuator coil	750 T
No of turns of AC magnet coil	700 T

bearings is suggested, along with a methodical design procedure [8].

Based on orientation, the AMB system could be either axial or radial. Here in this manuscript, an axial AMB system is discussed. To achieve contactless bearing systems, it is mandatory to levitate the rotor, and for that, some attraction force is needed which is provided by the electromagnetic coils which we call actuators [9]. An AMB system could consist of different types of coils and also different numbers of coils can be added and their overall effect on the system will be different in terms of high-speed application. In this manuscript, a comparative analysis is presented for I-shaped actuators when it is connected as a single coil and next as a double coil in the system [10]. As mentioned above, the controller plays an important role to control the levitation and speed of the rotor and so the article replicates the design aspects of the controller for both single- and double-coil arrangements [11]. After designing, both the systems are simulated as simulation software and implemented in hardware for the validation of simulation results. Finally, speed test is performed and compared the speed [12].

2 Overall system fabrication of I-type single-coil and double-coil active magnetic bearing for high-speed operation

Active magnetic bearing is an advanced technology in the high-speed rotating industry. For achieving a greater output, low loss and highly efficient machine design is necessary. We have better output in terms of high speed which we can get from the properly designed active magnetic bearing system. The design specification is given in Table 1 for single-coil and double-coil AMB systems. Three identical coils are designed for the single-coil and double-coil AMB to compare the performance between them [13–16].
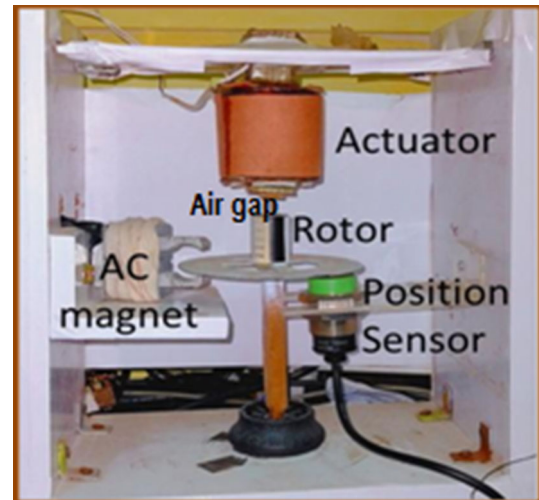

Fig. 2 Fabricated single-coil AMB system

According to the design data given in Table 1, two AMB systems are set up and presented below. Figure 2 represents the single-coil AMB, where a disc-type rotor is suspended below the actuator with support, the disc edge is placed in between the C-type AC magnet for the rotation, and a position sensor is placed below the rotor to sense the rotor position [17, 18].

Figure 3 represents the double-coil AMB, here also a similar type of orientation is there, only two I-type coils are used, and the rotor is placed in between them.

Active magnetic bearing system consists of the actuator, rotor, current sensor, current controller, position sensor, position controller, power amplifier, and AC magnet. The close-loop system of AMB is shown in Fig. 4. All the com-
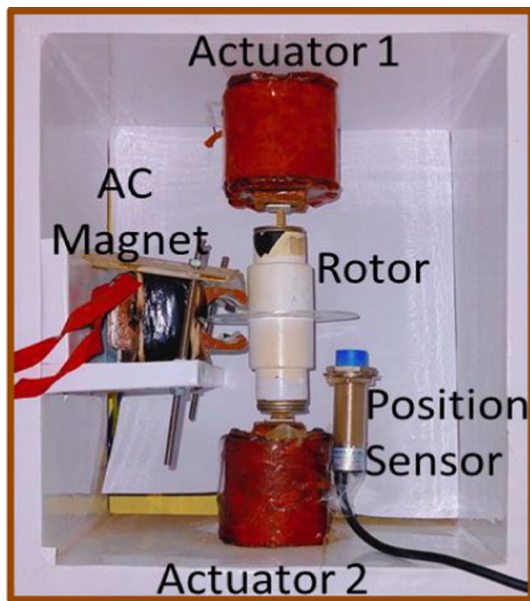
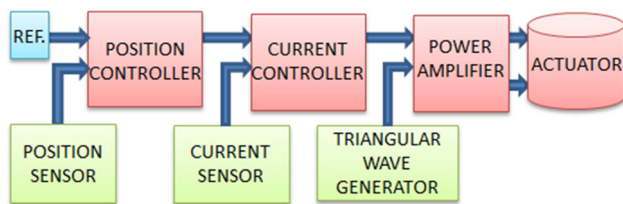**Fig. 3** Fabricated double-coil AMB system

Fig. 4 Block representation of complete AMB system

Table 2 Current sensor specification

Description	Ratings
Current transducer	LA 55 P
Supply voltage range	$\pm$ 12 V to $\pm$ 15 V
Primary current measuring range	$\pm$ 70A
Operating temperature range	$-$ 40 °C to 85 °C
Conversion ratio	1: 1000

the cylinder for rotational purposes. The rotor design parameters are presented in Table 1. Fabricated rotor for both the AMB systems i shown in Figs. 2 and 3.

2.3 Current sensor

Current sensors sense the current through the actuators at the time of the rotor levitated condition. The sensor signal is fed to the current controller to control the actuator coil current. Specification of the current sensor is given in Table 2.

2.4 Current controller

Current controller controls the current of the electromagnetic actuator and maintains the rotor levitated position. A controller, which may be proportional (P), proportional plus integral (PI), or proportional, integral, and differential (PID), is used to process the current error signal. The PI controller, which provides higher dynamic performance and ensures zero steady-state error, is the most often used controller among them. In this work, a proportional plus integral (PI) controller controls the coil current. The current controller's transfer function is provided by

$$G_{\mathrm{cc}}(s) = K_p + \frac{K_i}{s} \tag{1}$$

where K_P and K_i are the proportional and integral gains of the controller.

The actual current and the reference current are compared in the current control loop. A differential amplifier circuit receives the real current after scaling it (1 amp = 1 V) using a Hall-effect current sensor made by LEM. The reference current signal produced by the position controller output serves as the differential amplifier's additional input. A PI controller is used to process the differential amplifier's output current error signal.

The present controller's hardware design is depicted in Fig. 5, and its transfer function is described below.

$$G_{\mathrm{cc}}(s) = \frac{\left(R_6 + \frac{1}{sC_3}\right)}{R_5} = \left(\frac{R_6}{R_5} + \frac{1}{sR_5C_3}\right) \tag{2}$$
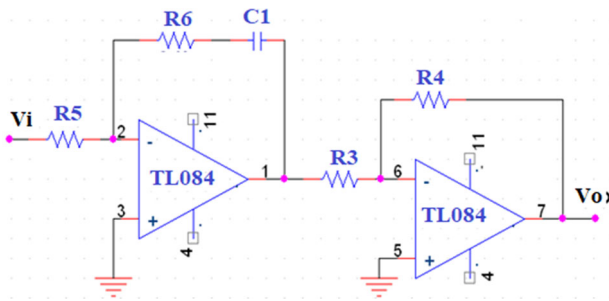
2.1 Actuator

Actuator is an important component of an AMB system that is responsible for moving or controlling the system. An actuator needs a control system to control the force to maintain the rotor's hovering position. The design data for the actuators used for both systems are presented in Table 1. According to the data presented in Table 1, the actuator for the single coil and double coil is fabricated and shown in Figs. 2 and 3.

2.2 Rotor

Rotor is an important component like the actuator, which is the only rotational part of the AMB system. The proper rotor design is important for better rotation. The rotor is constructed of two materials: An iron cylinder is used for attraction purposes, and an aluminium disc is attached below

Fig. 5 Designed circuit of PI controller

Table 3 Position sensor specification

Description	Ratings
Position sensor	Inductive sensor
Style	Cylinder shape
Sensing distance	0 to 10 mm
Shielded diameter	18 mm
Current output (DC/AC)	≤ 200 mA
Power supply	10 to 30 V DC
Ambient temperature	− 20 °C to + 70 °C

The proportional gain, when compared to the PI controller's standard form, $K_p = \frac{R_6}{R_5}$ and the integral gain,

Therefore, as per designed current (PI) controller

$$K_p = \frac{R_6}{R_5} = 4.724 \tag{3}$$

$$K_i = \frac{1}{R_5 C_3} = 1921.984 \tag{4}$$

$R_5 = 5.1k\,\Omega$ and $R_6 = 24.35k\,\Omega$.

Nearest standard values for resistors and capacitors have been taken into consideration for the current case. For adequate attenuation, which enables the control signal to vary within the height of the carrier signal, one additional level of gain and sign correction is necessary.

2.5 Position sensor

Inductive-type position sensor is used for the system. The position sensor senses the position of the rotor at the levitated condition and sends the feedback signal to the position controller to maintain the rotor position. Specification of the position sensor is given in Table 3.

2.6 Position controller

After receiving the signal from the position sensor, the position controller sends the current controller a signal that
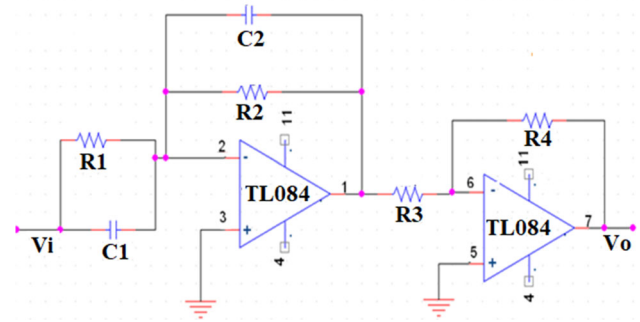
indicates whether the rotor is hovering or not. The controller design for the AMB system is given below, and the lead controller is employed as a position controller.

The system is unstable in an open loop with a pole $\left(+ \sqrt{\frac{K_x}{m}} \right)$ on the right half of the "s" plane, according to the transfer function of the plant.

$$G_p(s) = \frac{\Delta X(s)}{\Delta I(s)} = -\frac{\left(\frac{K_a}{m}\right)}{\left(s^2 - \frac{K_X}{m}\right)} \tag{5}$$

As position controllers, various classical controllers can be employed. The hardware circuit for the position controller employed in this work, which is essentially a phase lead compensator, is depicted in Fig. 6. The following is a description of the network's overall transfer function:

$$\frac{V_o(s)}{V_i(s)} = \frac{R_4 C_1}{R_3 C_2} \left(\frac{s + \frac{1}{R_1 C_1}}{s + \frac{1}{R_2 C_2}} \right) \tag{6}$$

The intended lead controller's transfer function at a 10-mm air gap is

$$G_{Lead}(s) = 12.24 \frac{(s + 45)}{(s + 526)} \tag{7}$$

Now comparing Eq. 6 and Eq. 7,

$$\frac{1}{R_1 C_1} = 45 \tag{8}$$

$$\frac{1}{R_2 C_2} = 526 \tag{9}$$

Let us assume, $C1 = C2 = 0.1\mu F$ and hence R1 comes out to be 222.22 KΩ and R2 = 19KΩ. The nearest standard values for resistors and capacitors have been taken into consideration for the current case.
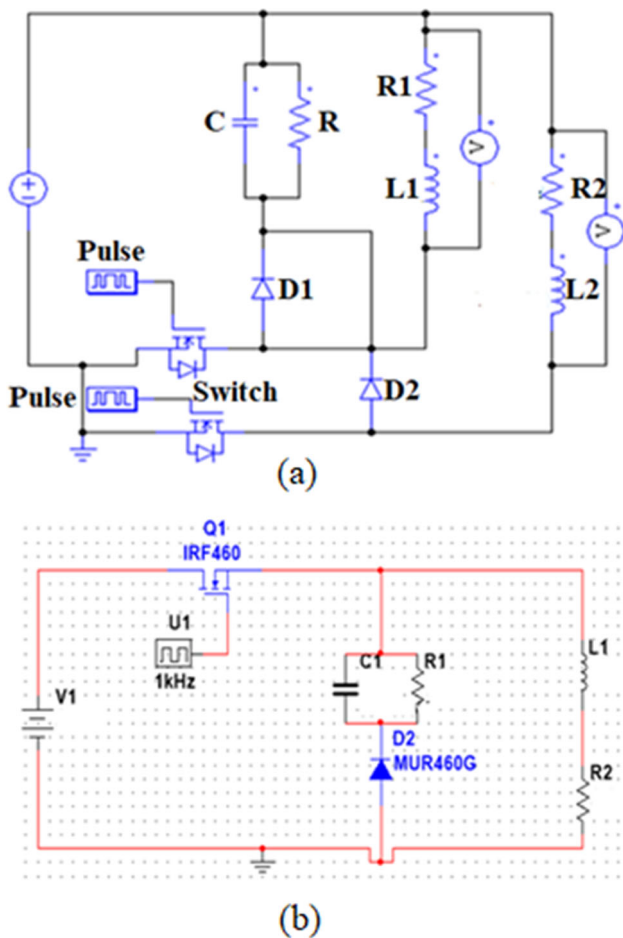

Fig. 6 Designed circuit of lead controller

(a)

(b)

Fig. 7 Power amplifier designed circuit for **a** double coil **b** single coil

2.7 Power amplifier

Power amplifier maintained the rotor levitated position by controlling the actuator coil current. Designed power amplifier circuit is presented in Fig. 7 for both the systems. The following transfer function can be used to describe the gain and time constant of the switching amplifier.

$$G_{ch}(s) = \frac{K_c}{1 + sT_c} \tag{10}$$

where K_{ch} is the gain and T_c is the time constant of the amplifier circuit.

The PI controller output is compared to a triangle wave whose instantaneous magnitude ranges between + 5 and -5 V to determine the chopper duty ratio. As long as the immediate magnitude of the PI controller output is greater than the instantaneous magnitude of the triangle wave, the chopper switches are on during each cycle. Half of the average carrier switching cycle time, or the time lag in the converter is defined in terms of the PWM switching frequency as $T_c = \frac{1}{2f_c}$; the converter's switching frequency in this instance
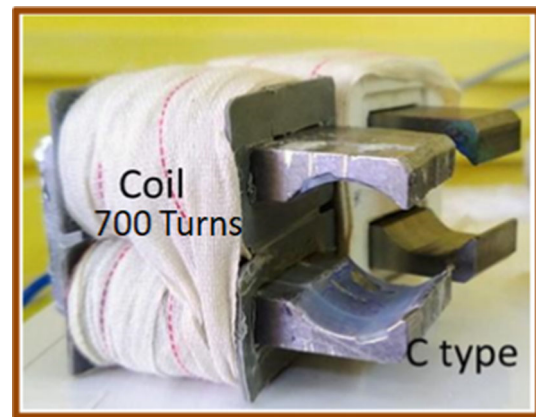
Fig. 8 Fabricated c-type AC magnet

is assumed 28 kHz. Due to the delay angle being approximately 0.018 ms, the chopper amplifier's transfer function is as follows:

$$G_{ch}(s) = \frac{20}{(1 + 0.000018s)} \tag{11}$$

The very short time constant is ignored, and the chopper's transfer function is reduced to a straightforward gain of 20.

2.8 AC magnet

AC magnets start functioning after the rotor levitation. This is the rotation system for the levitated rotor. Here a C-type AC magnet is introduced for the rotation. In this mechanism, the edge of the aluminium disc is placed inside the pole phase of the magnet, and after giving, the supply due to the electromagnetic induction disc will rotate. The fabricated C-type magnet is shown in Fig. 8.

3 Analysis of active magnetic bearing

Analysis of both systems is necessary to know the magnetic properties. Magnetic analysis has been performed using ANSYS MAXWELL finite element analysis software to find the flux, flux density, force, and inductance profile for different air gaps. All the parameters are compared between single-coil and double-coil systems.

ANSYS Maxwell analysis structure of both the systems is shown in Fig. 9. The magnetic analysis is performed for 10 different air gaps 1 mm to 10 mm.

Vector plot of magnetic intensity for the single coil and the double coil is presented in Figs. 10 and 11, for the equal current value applied to both the structures; H is 2.5407E + 04 A/m for the single coil and 2.4568E + 04 for the double coil.
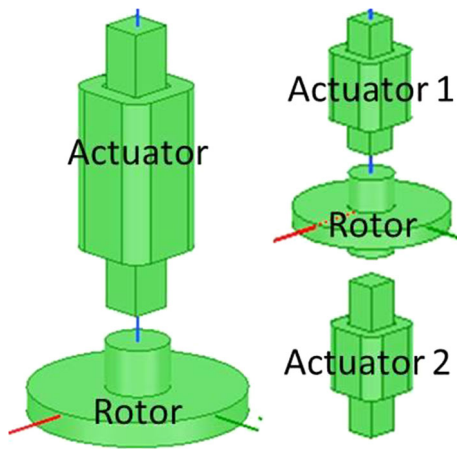
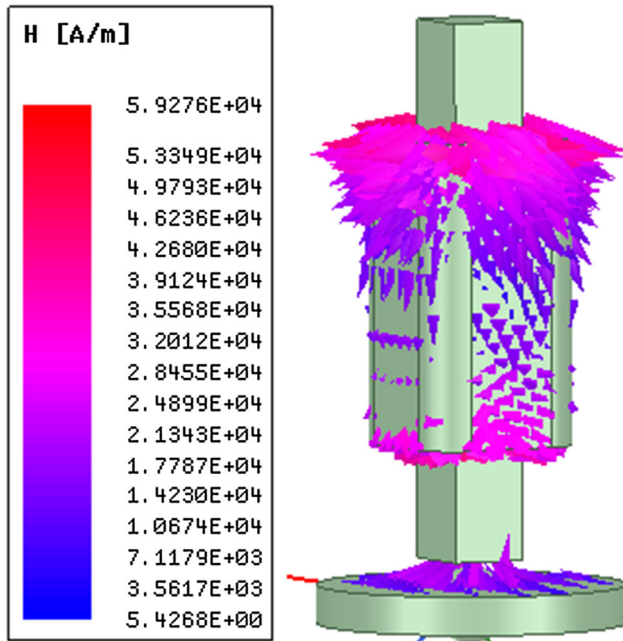**Fig. 9** I-type actuator and rotor structural model in ANSYS Maxwell for single coil and double coil

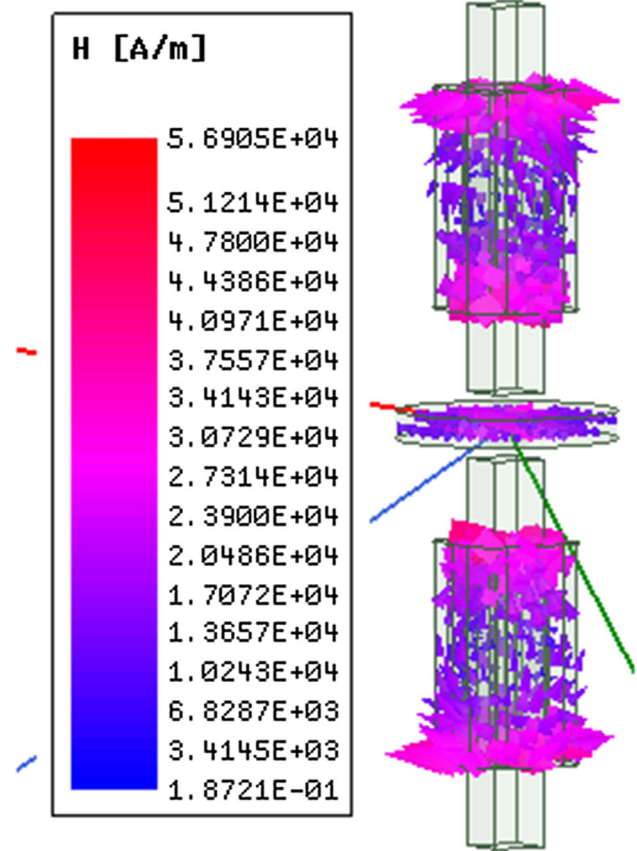**Fig. 10** Vector plot of magnetic intensity for single-coil AMB
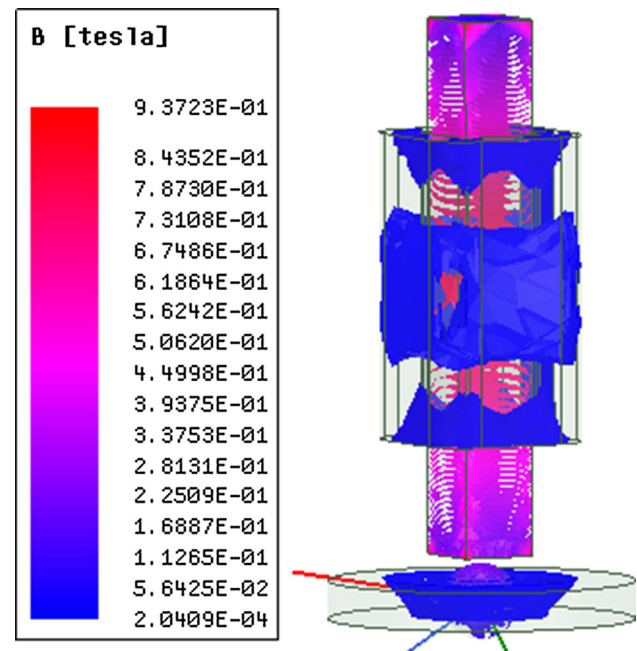

Fig. 11 Vector plot of magnetic intensity for double-coil AMB

Fig. 12 Magnitude of magnetic flux density for the single-coil AMB

Magnitude of magnetic flux density for the single coil and double coil is presented in Figs. 12 and 13, for the equal parameters applied to both the structures; B is 1.8526E-01 Tesla for single coil and 6.4568E-01 Tesla for the double coil.

Magnitude of current density for the single coil and double coil is presented in Figs. 14 and 15, for the equal parameters applied to both the structures; J is 2.8268E + 06 A/m^2 for single coil and 8.4468E + 06 A/m^2 for the double coil.

Vector plot of pulling force of electromagnetic actuator for the single coil and double coil is presented in Figs. 16 and 17, for the equal parameters applied to both the structures; F is 69.7506 Newton for single coil and 53.2654 Newton for the double coil.
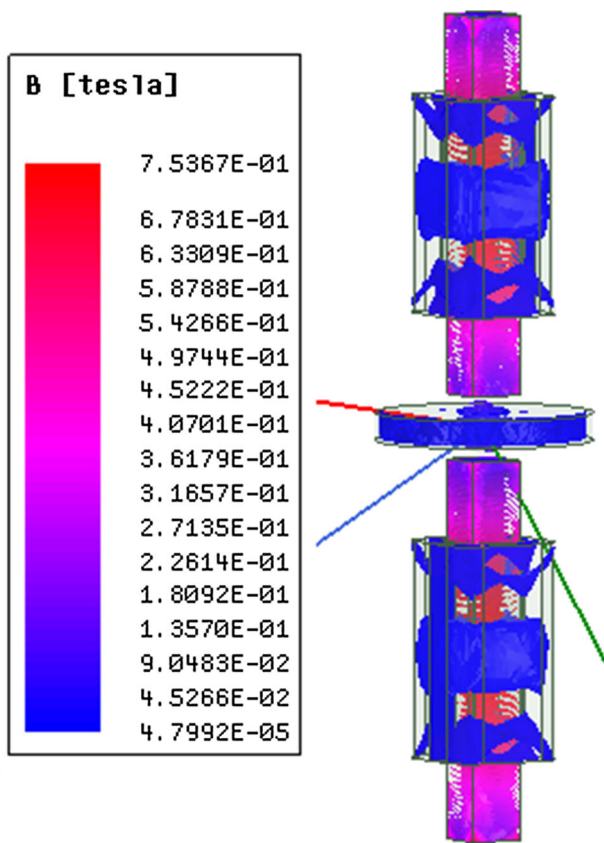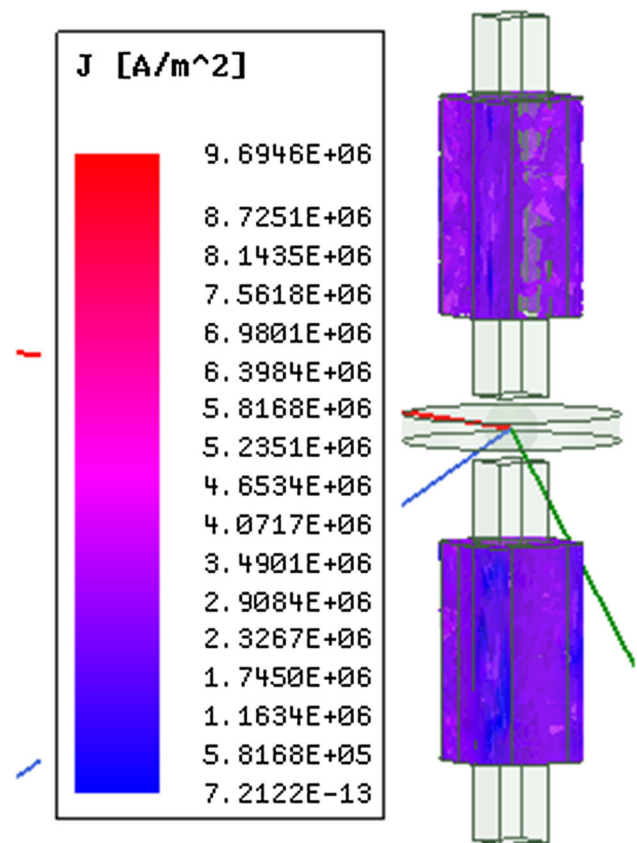
Fig. 13 Magnitude of magnetic flux density for the double-coil AMB

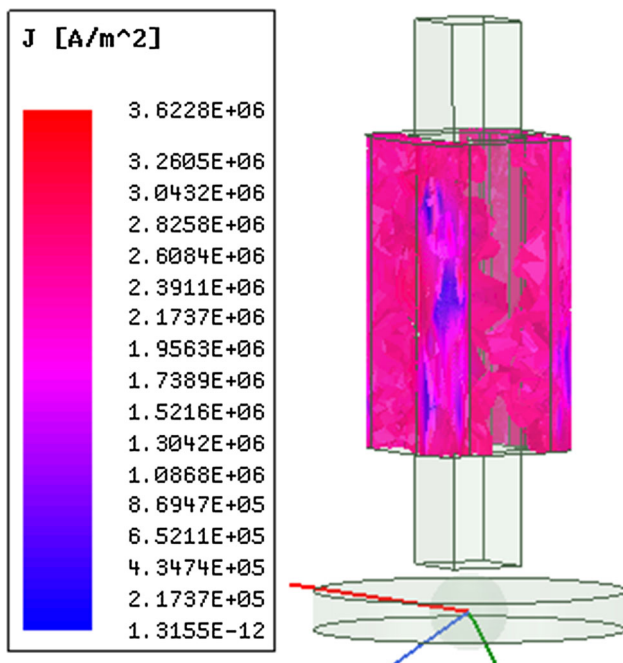**Fig. 15** Magnitude of current density for the double-coil AMB

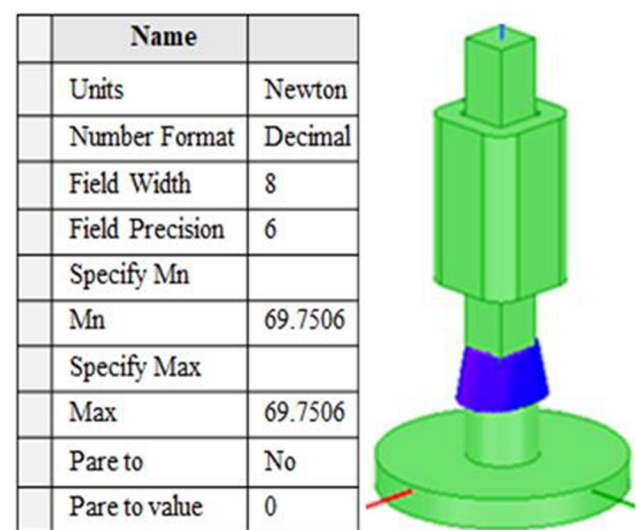**Fig. 14** Magnitude of current density for the single-coil AMB

Name	
Units	Newton
Number Format	Decimal
Field Width	8
Field Precision	6
Specify Mn	
Mn	69.7506
Specify Max	
Max	69.7506
Pare to	No
Pare to value	0

Fig. 16 Vector plot of pulling force of electromagnetic actuator for the single-coil AMB

Name	
Units	Newton
Number Format	Decimal
Field Width	8
Field Precision	6
Specify Mn	
Mn	53.2654
Specify Max	
Max	53.2654
Pare to	No
Pare to value	0
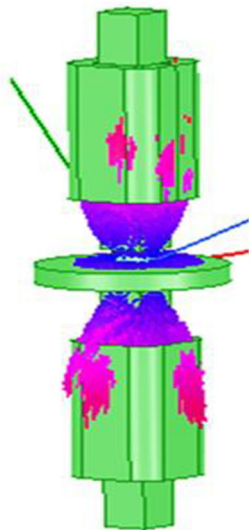
Fig. 17 Vector plot of pulling force of electromagnetic actuator for the double-coil AMB
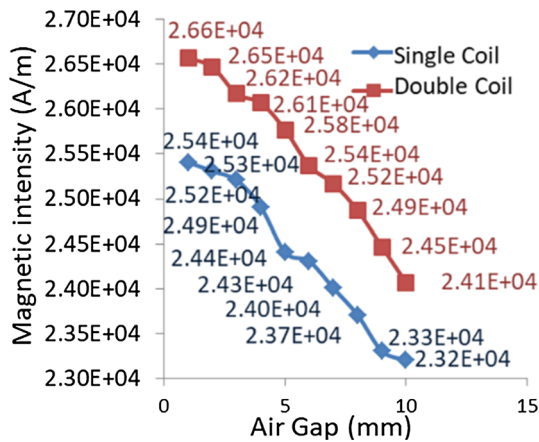

Fig. 18 Characteristics graph between magnetic intensity and air gap for single-coil and double-coil AMB

Fig. 19 Characteristics graph between flux density and air gap for both the system

Fig. 20 Characteristics graph between current density and air gap for single-coil and double-coil AMB

Fig. 21 Characteristics graph between pulling force, actuator, and air gap for single-coil and double-coil AMB

From the magnetic analysis, it is observed that the field intensity, magnetic flux density, current density are more in case of the double coil and pulling force is more in the single coil as there is no cancellation of force compared to the double coil.

Magnetic analysis results for 10 different air gaps for all the parameters are observed, and based on the data characteristics, graphs are drawn in between the single coil and double coil and presented in Figs. 18, 19, 20 and 21.

4 Simulation of single- and double-coil AMB

Simulation has been done for both the set-up before being implemented in hardware. Based on the RC value obtained
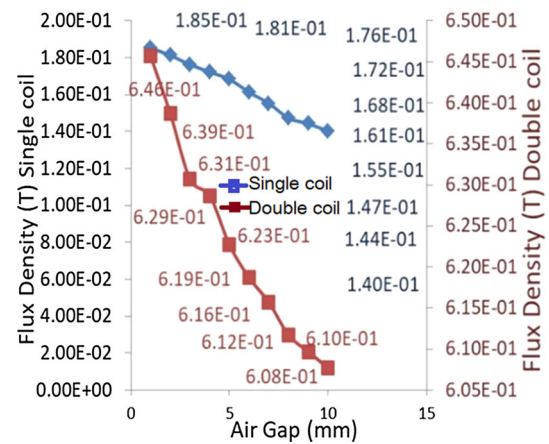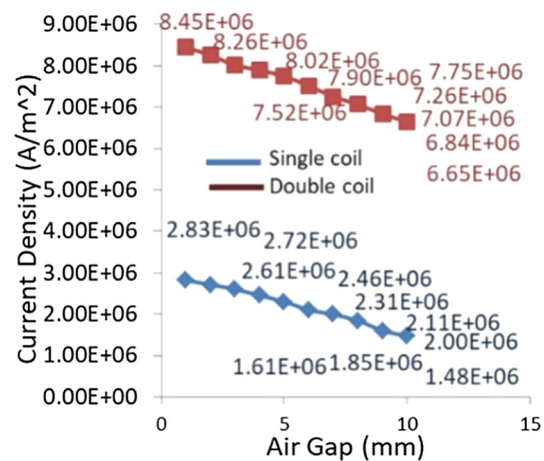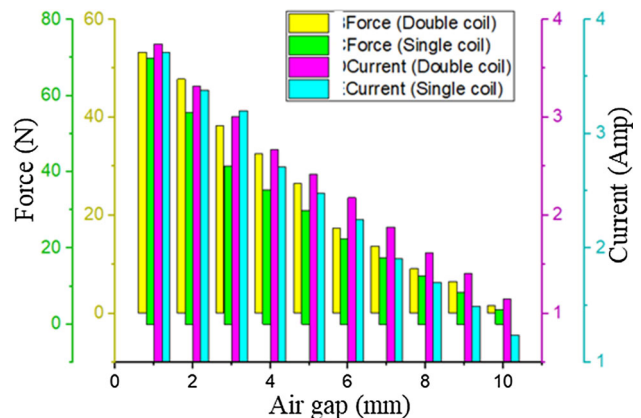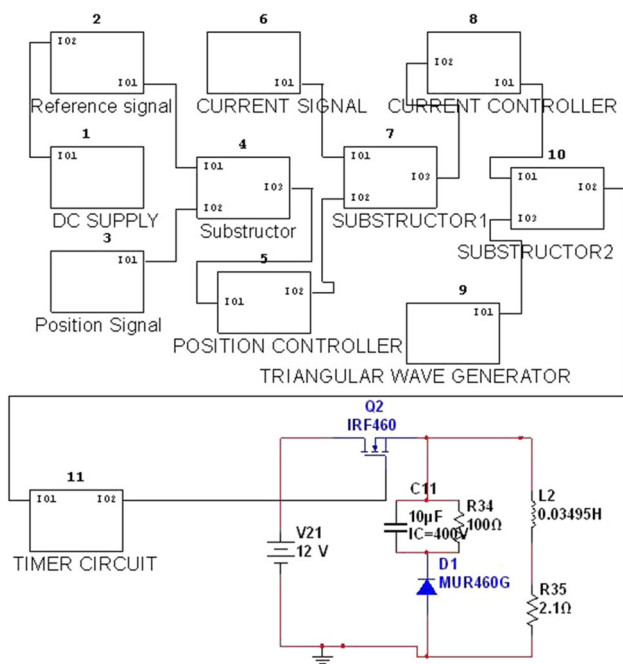
Fig. 22 Simulation circuit of a single-coil AMB system

Fig. 23 Simulation output for single-coil AMB system

Fig. 24 Simulation circuit of a single-coil AMB system
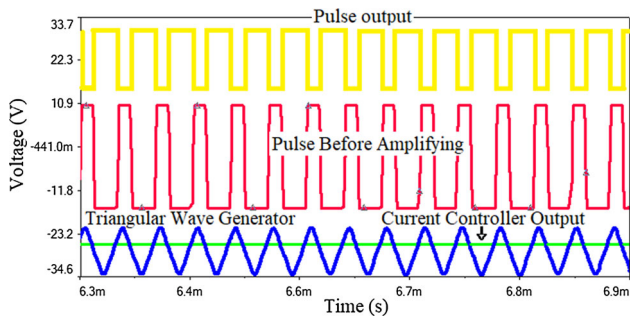

Fig. 25 Simulation output for single-coil AMB system

from the design, the simulation set-up is prepared in the simulation software and the outputs are observed.

4.1 Single-coil AMB

Simulation circuit for all the components of a single-coil AMB system is presented in terms of subsystem shown in Fig. 22, and the power amplifier circuit is shown where the gate pulse for the switch is obtained from the timer circuit. RL load is connected to the power amplifier circuit, and the rating of the RL load is obtained from the actuator coil.

Simulation output for a single coil is presented in Fig. 23. Pulse output before amplifying in red colour is obtained after comparing the current controller output in green colour with the triangular wave output in blue colour, and the amplified pulse output in yellow colour is achieved with the help of a timer circuit and fed to the switch of the amplifier.
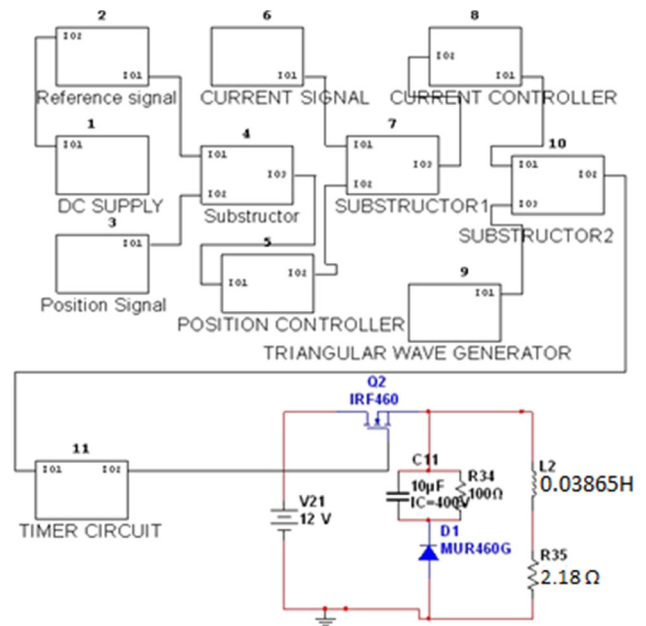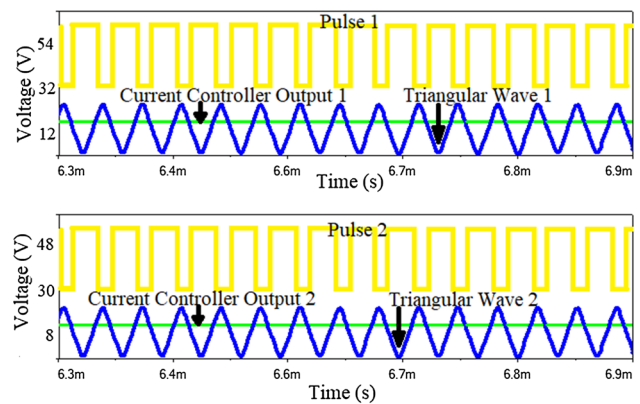
4.2 Double-coil AMB

The simulation circuit for the components used in the double coil AMB system is presented in terms of subsystems shown in Fig. 24; as both the coils are identical, only one simulation circuit is presented. The power amplifier circuit is shown where the gate pulse for the switch is obtained from the timer circuit. RL load is connected in the power amplifier circuit, and the rating of the RL load is obtained from the actuator coil.

Simulation output for the double coil is presented in Fig. 25. Pulse output in yellow colour is obtained after comparing the current controller output in green colour with the triangular wave output in blue colour, and the amplified pulse output in the black colour is achieved with the help of a timer circuit and fed to the switch of the amplifier.
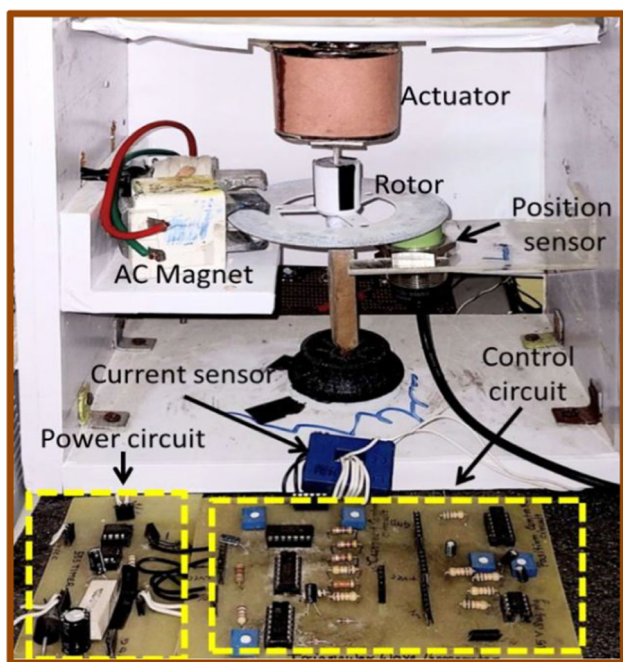
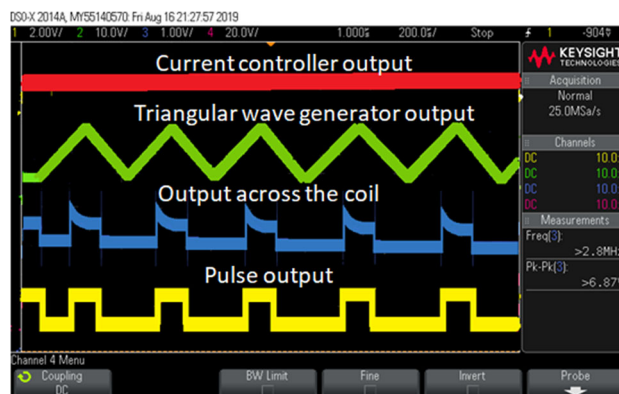**Fig. 26** Complete hardware system for the single-coil AMB system

Fig. 27 hardware output of current controller (red), triangular wave generator (green), output across the coil (blue) and pulse output (yellow) observed in the digital oscilloscope
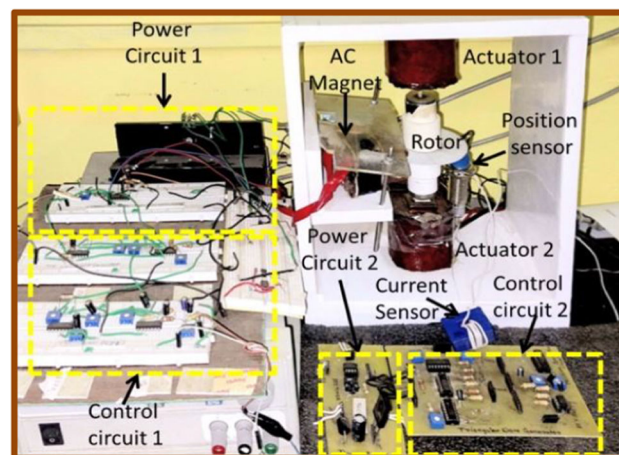
5 Experimental analysis of single- and double-coil AMB

Experimental analysis for both systems is necessary to validate the simulation results. Based on the simulation circuit, the hardware circuit is fabricated.

5.1 Single-coil AMB

Complete hardware system for single-coil AMB is shown in Fig. 26. In the hardware set-up, the disc-type rotor is suspended below the actuator coil, and according to the design data, hardware control circuit and power circuit is fabricated with the help of op-amp and r, c circuit. LEM 55 make current sensor is used for sensing the current of the actuator, and an inductive transducer-type position sensor is used to sense the position of the levitated rotor. After the levitation of the rotor, the output of each component is observed in the digital oscilloscope.

Observed hardware output of all the sections in the digital oscilloscope is presented in Fig. 27. The figure shows the current controller output, which is compared with triangular output, and the square wave output is obtained for triggering the MOSFET of the power amplifier. The output across the coil is observed and presented in the figure.

5.2 Double-coil AMB

Complete hardware system for double-coil AMB is shown in Fig. 28. In the hardware set-up, the disc-type rotor is sus-

Fig. 28 Complete hardware system for the single-coil AMB system

pended between the two-actuator coils, and according to the design data, hardware control circuit and power circuit is fabricated for both the actuator with the help of the r, c circuit, an op-amp. Two LEM 55 make current sensors are used for sensing the current of actuators, and an inductive-type position sensor is used to sense the position of the levitated rotor. After the levitation of the rotor, the output of each component is observed in the digital oscilloscope.

Observed output of all the sections in the digital oscilloscope for both the actuators is presented in Fig. 29. The figure shows the current controller output, which is compared with triangular output, and the square wave output is obtained for triggering the MOSFET of the power amplifier. The output across the coil is observed and presented in the figure.

Hardware output is compared with the simulation output, and similar type of output has been observed in both the cases.
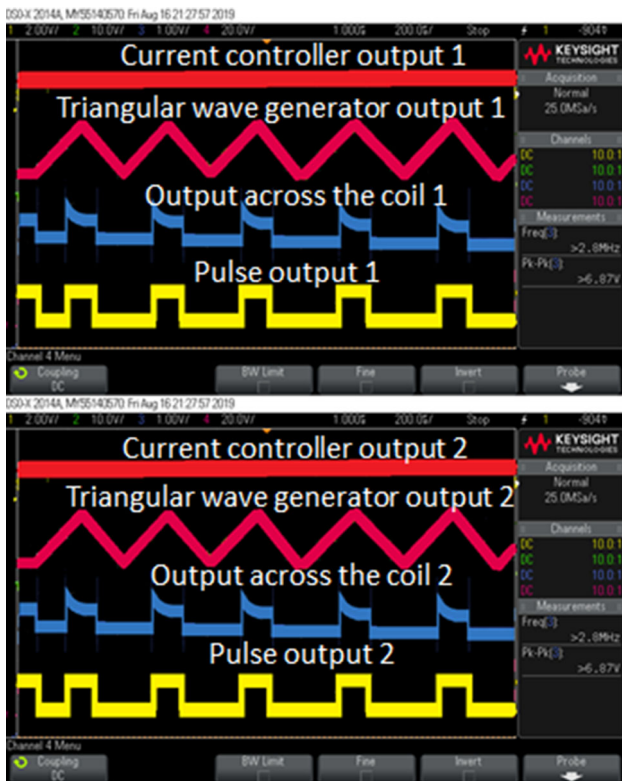
Fig. 29 Hardware output of the current controller (red), triangular wave generator (pink), output across the coil (blue), and pulse output (yellow) for both the coil is observed in the digital oscilloscope

6 Speed test of single-coil and double-coil AMB

Levitated rotor is placed in between the pole phase of the c-type AC magnet as shown in Fig. 21. This will help the rotor to rotate, and the rotational speed is depending on the supply voltage. Ten different voltages across the AC magnet speed are observed in both the system, and the data are presented in Table 4. The performance graph for both systems is presented in Fig. 30. For a single coil at a 10 V supply voltage of 4234 rpm and for a 100 V supply, 22,425 rpm is observed, and for a double coil 3746 rpm at a 10 V supply and for a 100 V supply, 19,873 rpm is observed. From the speed test, it is noticed that for single coil high speed is obtained compared to double-coil AMB.

Table 4 Rotational speed of both the systems for ten different voltages across the AC magnet

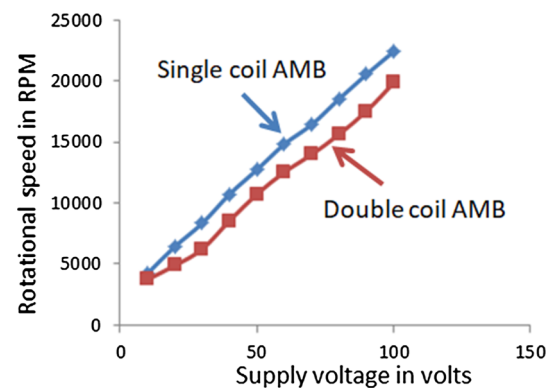| Supply voltage	RPM for single-coil AMB	RPM for double-coil AMB
10	4234	3746
20	6443	4886
30	8345	6233
40	10,736	8563
50	12,734	10,736
60	14,833	12,536
70	16,438	13,986
80	18,535	15,636
90	20,546	17,535
100	22,425	19,873

Fig. 30 Performance graph of rotational speed for both systems for different supply voltages

7 Conclusion

This manuscript explains the design for achieving higher rotational speed to meet the industrial need. For both the system, PI and lead controllers are used as current and position controllers. An economical single-switch power amplifier is used to control the actuator current to maintain the rotor levitation. According to the design, data simulation is done in Multisim software, and after simulation, the system is implemented in hardware and compared the results between I-type single- and double-coil AMB. Finally, the levitated rotor is rotated using a rotational system and speed is measured using a tachometer. For double coil 19,873 rpm and single coil, 22,425 rpm speed is achieved.

Declarations

References

1. Smirnov A, Uzhegov N, Sillanpää T, Pyrhönen J, Pyrhönen O (2017) High-speed electrical machine with active magnetic bearing system optimization. IEEE Trans Industr Electron 64(12):9876–9885
2. Gerada D, Mebarki A, Brown NL, Gerada C, Cavagnino A, Boglietti A (2014) High-speed electrical machines: technologies, trends, and developments. IEEE Trans Industr Electron 61(6):2946–2959
3. Papini L, Raminosoa T, Gerada D, Gerada C (2014) A high-speed permanent-magnet machine for fault-tolerant drivetrains. IEEE Trans Industr Electron 61(6):3071–3080
4. S. Debnath, P. K. Biswas and J. Laldingliana, "Analysis and simulation of PWM based power amplifier for single axis Active Magnetic Bearing (AMB)," In: *2017 IEEE transportation electrification conference (ITEC-India)*, Pune, 2017, pp. 1-5
5. Laldingliana J, Debnath S, Biswas PK (2023) Design and speed control of U-type 3-coil active magnetic bearing. Electr Eng. https://doi.org/10.1007/s00202-023-01838-y
6. Zansong Fu, Dong Jiang and Ronghai Qu, "Design of four-axis magnetic bearing for high speed motor," 2016 IEEE 8th International Power Electronics and Motion Control Conference (IPEMC-ECCE Asia), 2016, pp. 786–791, doi: https://doi.org/10.1109/IPEMC.2016.7512385.
7. Schuck M, Nussbaumer T, Kolar JW (2016) Characterization of Electromagnetic Rotor Material Properties and Their Impact on an Ultra-High Speed Spinning Ball Motor. IEEE Trans Magnet 52(7):1–4. https://doi.org/10.1109/TMAG.2016.2529498
8. Kurvinen E et al (2021) Design and manufacturing of a modular low-voltage multimegawatt high-speed solid-rotor induction motor. IEEE Trans. Industry Appl. 57(6):6903–6912. https://doi.org/10.1109/TIA.2021.3084137
9. Kanebako H, Okada Y (2003) New design of hybrid-type self-bearing motor for small, high-speed spindle. IEEE/ASME Trans Mechatron 8(1):111–119
10. Debnath S, Biswas PK (2021) Design, analysis, and testing of I-type electromagnetic actuator used in single-coil active magnetic bearing. Electr Eng 103:183–194
11. Wong TH (1986) Design of a Magnetic Levitation Control System???An Undergraduate Project. IEEE Trans Educ 29(4):196–200
12. Asama J, Asami T, Imakawa T, Chiba A, Nakajima A, Rahman MA (2011) Effects of permanent-magnet passive magnetic bearing on a two-axis actively regulated low-speed bearingless motor. IEEE Trans Energy Convers 26(1):46–54
13. Das U, Debnath S, Gupta S, Biswas PK, Babu TS, Nwulu NI (2023) "Active Magnetic bearing system using I-type and U-type actuator. IEEE Access. https://doi.org/10.1109/ACCESS.2023.3276324
14. Wang K, Ma X, Liu Q, Chen S, Liu X (2019) Multiphysics global design and experiment of the electric machine with a flexible rotor supported by active magnetic bearing. IEEE/ASME Trans Mechatron 24(2):820–831
15. Debnath S, Biswas PK (2020) Advanced magnetic bearing device for high-speed applications with an I-type electromagnet. Electric Power Compon Syst 48(16–17):1862–1874
16. Cole MOT, Fakkaew W (2018) An active magnetic bearing for thin-walled rotors: vibrational dynamics and stabilizing control. IEEE/ASME Trans Mechatron 23(6):2859–2869
17. Huang Z, Fang J (2016) Multiphysics design and optimization of high-speed permanent-magnet electrical machines for air blower applications. IEEE Trans Industr Electron 63(5):2766–2774
18. Debnath S, Biswas PK (2021) Study and analysis on some design aspects in single and multi-axis active magnetic bearing (AMB). J Appl Res Technol 19(5):448–471